Approximate Expressions for the Magnetic Potential and Fields of Two-Dimensional, Asymmetrical Magnetic Recording Heads

Mustafa M. Aziz, Ammar I. Edress, and C. David Wright

College of Engineering, Mathematics and Physical Sciences, University of Exeter, Exeter EX4 4QF, United Kingdom

Two-dimensional asymmetrical magnetic head are characterised by parallel inclination of the semi-infinite, inner gap walls, and where the gap length and head-to-underlayer separation are small compared to the other dimensions in the head. With head corner inclination, these structures contribute to reduction in the effective gap length of the head and therefore increase in the field magnitude and narrowing of the field distributions near the acute gap corner. Asymmetrical heads were therefore proposed for increasing the writing and readout resolutions in gapped magnetic head structures. There are currently no explicit or approximate analytical solutions for the potential and fields from two-dimensional asymmetrical magnetic heads. This paper is concerned with the detailed theoretical derivation of relatively simple closed-form approximations for the scalar magnetic potential and fields from two-dimensional asymmetrical magnetic heads and their Fourier transforms, applicable to any arbitrary corner inclination angle. A general theory based on the translated Sine Fourier series is developed to model and study the reaction of a soft magnetic underlayer (SUL) on the surface potential of any magnetic head structure, and applied to the asymmetrical head. The approximate potential and field expressions derived in this paper demonstrated very good agreement with finite-element calculations of two-dimensional asymmetrical heads.

***Index Terms*— Magnetic recording, asymmetrical heads, Laplace's equation, Fourier series, magnetic fields.**

I. Introduction

The magnetic head is an integral part of magnetic recording systems. The head geometry and dimensions determine the magnitude and distribution of the fringing gap fields and their gradients, therefore affecting the size and shape of the recorded magnetisation pattern in the magnetic medium during recording, and the resolving performance of the head in readout [1]. The design of magnetic heads therefore has direct impact on the achievable storage density of magnetic recording systems.s.

Conventional two-dimensional magnetic heads, including the ring-type, finite-pole thin-film and single pole head structures have symmetrical pole geometry and produce mostly symmetrical fringing fields in the gap or pole corner regions. Asymmetric heads differ by rotating, in parallel, the pole corners in the gap region through exterior angle θ as indicated in two-dimensions in Fig. 1, where the x-axis is the direction along the head/medium motion, and the y-axis is normal to the head surface. In this two-dimensional geometry, the cross-track direction (along z-axis) is assumed much larger in extent compared to the gap length g and head-to-underlayer separation d.

Corresponding author: Mustafa M. Aziz (e-mail: M.M.Aziz@ex.ac.uk).

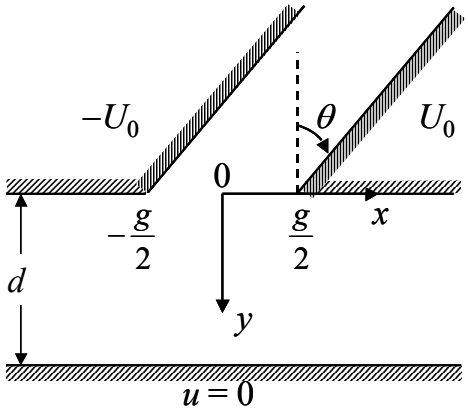

Fig. 1. Two-dimensional geometry of the asymmetrical head, with gap length g and exterior corner inclination angle θ. The poles are assumed to have infinite permeability and therefore with equipotentials $\pm U_0$, at a distance d from a soft magnetic underlayer (SUL) held at zero potential. To model two-dimensional heads without an underlayer, the SUL is removed with $d \to \infty$.

The significance of the asymmetrical head shown in Fig. 1 arises from the increased magnetic charge density in the acute head corner [2]. This leads to an increase in the magnitude of the magnetic fields in this region and narrowing of their distributions as will be shown later in this article. Asymmetric heads were therefore proposed for increasing the recording resolution in longitudinal and perpendicular recording due to the increased field gradients near the acute pole corner in the gap region [3]. Asymmetrical heads were also suggested as a method of increasing the readout resolution of ring-type inductive heads and develop 'gap-null free' heads [4], primarily through the natural reduction in the 'effective' gap length of the head with the increase in θ enabling shorter recorded magnetisation patterns in the recording medium to be resolved. Asymmetric head designs were also incorporated in perpendicular heads with tapering in both the main pole and side shields to increase the recording fields and their gradients

This article has been accepted for publication in a future issue of this journal, but has not been fully edited. Content may change prior to final publication. Citation information: DOI 10.1109/TMAG.2015.2492947, IEEE Transactions on Magnetics

and to reduce side fringing [5]. This tapered single-pole head structures with tapered shields, incorporating the asymmetric gapped geometry, were also investigated as part of corner-type head designs for high-resolution, two-dimensional magnetic recording [6].

There are currently neither explicit nor approximate expressions for the potential and fields for asymmetrical magnetic recording heads. Therefore the explicit functional dependence of the corresponding magnetic fields' magnitude, gradient, and wavelength response on the head parameters (such as θ, g and d) is not well understood. The difficulty in deriving explicit solutions for the potentials and fields of asymmetrical heads arises from the fact that the geometry does not conform to conventional coordinate systems, for which formal methods of solution can be applied. Implicit, conformal mapping solutions were previously derived exactly for asymmetrical heads, but only for limited (rational) corner angles [7,8]. Conformal mapping solutions require numerical inversion to explicitly determine the vector fields in the space surrounding the head surface, and are thus not practical to use in head design and optimisation studies, nor in more complex simulations of the record and readout processes. This paper therefore provides, for the first time, a detailed and comprehensive derivations of relatively simple analytical approximations for the magnetic scalar potential and fields from asymmetrical heads with and without a soft magnetic underlayer (SUL), for any exterior corner inclination angle θ (0° to 90°).

Fields from magnetic heads can be derived from the solution of the boundary value problem involving Laplace's equation for the scalar magnetic potential, u, which in two-dimensions is written as:

$$\frac{\partial^2 u}{\partial x^2} + \frac{\partial^2 u}{\partial y^2} = 0 \qquad (1)$$

using the assumption that the head pole pieces are infinitely permeable, thus providing the equipotential boundaries for this system. The magnetic fields $\boldsymbol{H}$ are then determined from the gradient of the potential $\boldsymbol{H} = -\nabla u$. It is generally difficult to derive explicit and exact solutions to Laplace's equation for the common two-dimensional magnetic head geometries directly. The rigorous approach has been to divide the head into rectangular regions inside the gap and beyond the head poles, and derive general solutions for the scalar potential in these regions in the form of an infinite Fourier series. Forcing the continuity of potentials and normal fields at the interfaces between these rectangular regions enables the determination of the Fourier coefficients. The few exact solutions derived this way are for conventional symmetrical (right-angled) head structures including the ring-type head [9,10], single pole and perpendicular heads [11,12], and their shielded varieties [13]. The Fourier coefficients [11,14] in these series solutions are normally determined implicitly from the solution of a large system of linear equations and involve numerical integration, which complicates the evaluation of the magnetic potentials and fields. An alternative approach for mapping the magnetic fields from two-dimensional head structures involves explicitly specifying the potential or the field distribution along the head surface, and convolving this distribution with the appropriate Green's function for the specific geometry and boundary conditions of the problem to obtain the potential and fields everywhere beyond the head surface. The accuracy of this method relies heavily on the accuracy of the assumed surface potential or field. The well-known Karlqvist approximation [15] for example, assumes a linear gap surface potential following the potential deep inside the gap in a ring-type head, to predict simple and convenient closed-form expressions for the fields beyond the head surface. One approach that has been adopted for the determination of more accurate surface field distributions is through assuming a plausible rational function approximation for the surface fields in the gap region and beyond pole corners, with adjustable coefficients that are determined through fitting to computer models of the magnetic head (such as finite-elements) (for example ref. [16]). These simplified rational function approximations are then convolved with the appropriate Green's functions to determine the fields everywhere beyond the head surface. In this article, a combination of the aforementioned methods will be used to arrive at explicit and approximate closed-form expressions for the potential and fields for two-dimensional asymmetrical heads as outlined next.

Asymmetrical heads exhibit non-equal surface charge distributions in the pole corner, leading to asymmetry in the gap surface potential. In this paper, this asymmetry in head surface potential is modelled, in the absence of a SUL, using a rational function approximation, derived from analysis of finite-element solution to Laplace's equation for this geometry at different corner angles θ in the range $0^o \rightarrow 90^o$. The approximate surface potential is then convolved with the Green's function solution for the semi-infinite, two-dimensional geometry considered here to determine the potential and fields everywhere beyond the surface of the head. In the presence of a SUL, a general and approximate theory, based on the integral transform method, for any two-dimensional gapped head structure is developed to approximate the reaction of the high permeability underlayer on the known head surface potential in the absence of the underlayer. This modified surface potential is then convolved with the two-dimensional Green's function for the head/underlayer combination to determine the fields everywhere beyond the head surface. The Fourier transform of the asymmetrical head surface field, in the presence and absence of a SUL, is also derived exactly to study the effect of corner angle inclination on the wavelength response of asymmetrical heads.

This article has been accepted for publication in a future issue of this journal, but has not been fully edited. Content may change prior to final publication. Citation information: DOI 10.1109/TMAG.2015.2492947, IEEE Transactions on Magnetics

For the mathematics to remain analytical and tractable, the theory presented here is for two-dimensional head structures with infinite-cross track width, and based on magnetostatics. Therefore transient effects are neglected, and the effects of finite-track width of the head are not considered. Increasing the exterior angle θ increases the magnetic flux density in the acute head corner, leading to corner saturation that occurs at lower driving fields compared to right-angled corners. Pole saturation affects the gradient of the fields and degrades the recording performance especially at small head-to-recording medium separations [18]. Studying and modelling pole saturation in asymmetrical heads and in the SUL requires a full numerical treatment, which is beyond the scope and length of this theoretical article. Corner saturation in asymmetrical heads was examined numerically using finite-elements in two-dimensions in [19] using linear and nonlinear B-H models of the field dependance of permeability for low saturation MnZn ferrites. Saturation was induced with a deep-gap driving field greater than half the saturation magnetisation of the core material [18]. Their study showed that severe saturation occurred for inclination angles $\theta > 40°$ causing large reductions in the magnitude of the fields near the acute corner of the head (when compared to the infinite permeability model).

To study the validity of the approximate models and estimate the errors in the approximations, Laplace's equation was solved in two dimensions numerically using finite-elements on Comsol Multiphysics®[17]. The geometry and boundary conditions used in the finite-element simulations follows from Fig. 1, with the simulation space terminated by zero potential planes at very large distances from the gap region to model semi-infinite head structures in the absence of an underlayer, or with the zero potential plane at a distance d from the head surface in the presence of an underlayer. Adaptive and progressive mesh refinement was employed in the boundaries near the head corners to increase the mesh resolution in the (tilted) corner regions to accurately evaluate the potentials and fields.

In this article, the closeness of the approximate potential and field models to the more accurate finite-element calculations is estimated using the absolute root-mean-square deviation (RMSD), defined as:

$$\mathrm{RMSD} = \sqrt{\frac{1}{\mathrm{N}}\sum_{n=1}^{N}\left(\hat{f}_n - f_n\right)^2}$$

where $\hat{f}_n$ is the approximated model value, f_n is the finite-element data and the summation is taken over N data points. The RMSD is a global, absolute measure with the same units as the potential or fields used in the estimation, with lower values indicating less deviation from the accurate finite-element simulations. The RMSD will therefore be normalised by the extrema in the potential or field magnitudes to estimate the percentage deviation.

This article will begin with the derivation of the rational function approximation for the surface potential for two-dimensional asymmetrical heads in the absence of a SUL in Section II. The integral transform approach is used in the same section to derive a general theory for modelling the reaction of the underlayer on the surface potential. The surface potentials are then used in Section III along with the two-dimensional Green's functions to derive expressions for the magnetic fields beyond the head surface. In Section IV and before concluding this article, the Fourier transform of the surface fields is derived to explore the effect of asymmetry on the wavelength content of the fields. The validity of the approximate magnetic potential and field models, their limitations and improvements are discussed in the relevant sections of the article.

II. Surface Potential Approximations

In this section, approximate expressions are derived for the surface magnetic potential for asymmetrical heads with and without a SUL. These will be later convolved with the Green's function for the magnetic head geometry to determine the potentials and fields everywhere beyond the head surface.

A. Without underlayer

The gap surface potential for an asymmetrical head calculated using finite-elements is shown Fig. 2 for a number of exterior corner angles θ. For right-angled corners ($\theta = 0°$), the gap potential is symmetrical with increasing gradient (and therefore fields) near the gap corners at $\pm g/2$ [1]. Increasing θ increases the asymmetry in the potential due to the increased magnetic surface charge density in the acute corner at $x = g/2$, and shifts the zero-crossing of the potential towards this corner. This displacement of the potential zero-crossing leads to a reduction in the effective gap length of the head. In the limit where $\theta \to 90°$, the effective gap length reduces to zero towards the right corner with a step change in the surface potential at $x = g/2$, leading to the narrow gap or far field potential distribution [1].

This article has been accepted for publication in a future issue of this journal, but has not been fully edited. Content may change prior to final publication. Citation information: DOI 10.1109/TMAG.2015.2492947, IEEE Transactions on Magnetics

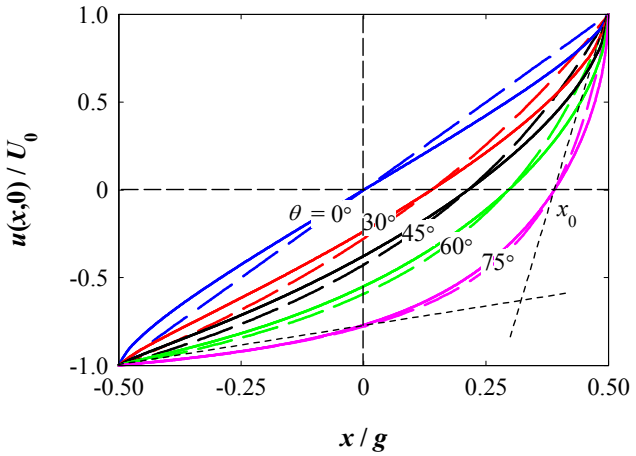

Fig. 2. Calculated gap surface potential using finite-elements (solid lines) and the approximate surface potential in (2) and (3) (dashed lines) for different corner angles. The dotted straight lines highlight the approximate hyperbolic locus of the asymmetrical potential, and were used as guides to derive the rational function approximation for the potential.

The surface gap potential determined by finite-elements in Fig. 2 may be characterised by both: (i) a shift in the zero-crossing, x_0, of the potential, and (ii) scaling of the potential magnitude and gradient near the origin, with changes in exterior corner angle θ. This surface gap potential approximately traces a hyperbola joining the two intersecting straight dashed lines indicated in Fig. 2 (shown for $\theta = 75°$ as an example). Thus, the gap surface potential may be described using the following rational function:

$$u(x,0) = a + \frac{b}{c + x}$$

The constants a, b and c were determined by requiring that the potential satisfies the conditions $u = \pm U_0$ at $x = \pm g/2$, and that the potential vanishes at $x = x_0$ where x_0 is a function of θ. This yields the following approximate surface potential:

$$u(x,0) = \begin{cases} -U_0 & x < -g/2 \\ \dfrac{g}{2}\dfrac{U_0(x - x_0)}{(g^2/4 - x_0 x)} & -g/2 \le x \le g/2 \\ U_0 & x > g/2 \end{cases} \qquad (2)$$

The potential in (2) is continuous and differentiable over the gap length, therefore satisfying the continuity requirement of the potential and fields in the gap. When $\theta = 0°$ (and $x_0 = 0$) the head is symmetrical, and the gap potential in (2) reduces to the linear (Karlqvist) approximation [16]. As $\theta \to 90°$ (and $x_0 = g/2$), equation (2) produces a step function change in the potential along the head surface at $x = g/2$ to model the narrow gap head.

The dependence of the shift in the zero-crossing of the gap potential, x_0, on corner angle θ was determined from the finite-element calculations and is shown in Fig. 3 (open circles). The tangent function was found to provide the best least-squares fit to this dependence using the following fitting parameters:

$$\frac{x_0}{g} = 0.564 \tan(0.462\theta) \quad 0 \le x_0 \le g/2\,, \quad 0 \le \theta \le \pi/2 \qquad (3)$$

Equation (3) is illustrated in Fig. 3 (solid line) with a very small absolute RMS deviation of 3.71×10^{-4} from the finite-element data. Therefore (3) will be used subsequently in this article for the determination of x_0 for a given corner angle θ.

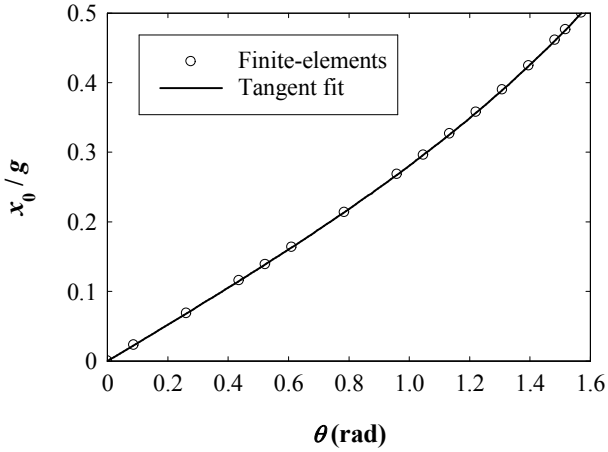

Fig. 3. Dependence of the zero-crossing shift of the gap potential, x_0, on the corner angle θ, determined from the finite-element solution of Laplace's equation (circles). The solid line shows the least-squares fitting to the finite-element data using the tangent function with best fit parameters: $x_0/g = 0.564\tan(0.462\theta)$.

The approximate surface gap potential in (2) is plotted in Fig. 2 (dashed lines) using the calculated values of x_0 from (3), showing good agreement with the finite-element potential for different values of θ. Fig. 4 shows the RMSD between the approximate potential and finite-element calculations, normalised by the maximum change in the gap potential ($2U_0$), as a function of exterior corner angle. For small θ, the RMSD is 3.3% which is consistent with the error in the Karlqvist approximation for symmetrical heads. The RMSD reduces (and therefore accuracy increases) with increasing θ and correctly vanishes as $\theta \to 90°$ (narrow gap limit). Another advantage of the surface potential approximation in (2) is that it enables the derivation of exact, and relatively simple, closed-form solutions for the potential and fields everywhere beyond the head surface as illustrated later in this article.

This article has been accepted for publication in a future issue of this journal, but has not been fully edited. Content may change prior to final publication. Citation information: DOI 10.1109/TMAG.2015.2492947, IEEE Transactions on Magnetics

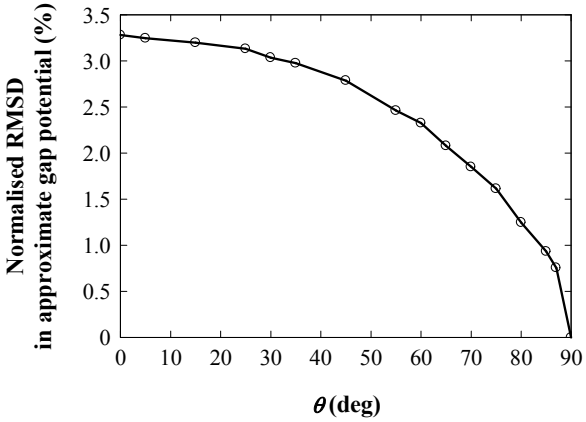

Fig. 4. The RMSD between the approximate gap potential in (2) and the finite-element calculations, normalised by maximum change of potential in the gap ($2U_0$), as a function of the exterior corner angle θ. This plot shows the increase in accuracy of the rational function approximation for the surface potential with increasing θ.

B. With underlayer

The presence of a SUL modifies the magnetic circuit of the head and the distribution of the head surface potential [20]. The reaction of the underlayer on the surface potential for an asymmetrical head with θ = 45° is illustrated in Fig. 5, calculated using finite-elements (solid lines) for different head-to-underlayer spacings. This figure shows that the effect the underlayer is more prominent for small head-to-underlayer separations $d/g < 0.5$, resulting in the reduction of the surface potential and its gradient in the gap central region, while increasing the potential gradient near the gap corners. With increasing the head-to-underlayer separation to values of $d/g >$ 0.5, the surface potential rapidly approaches the surface potential without an underlayer. The same behaviour applies to other exterior corner angles, with the added displacement of the zero-crossing of the potential towards the acute corner with increasing θ, as previously described for the case without an underlayer.

Modelling the reaction of the underlayer on the head surface potential is complex due to the presence of finite-boundaries in this problem. Theoretical developments commonly use the surface potential or surface field of magnetic heads in the absence of the underlayer, as an approximation, along with the appropriate Green's functions to determine the potential and fields everywhere beyond the head surface (for example [21]). It will be shown in this article that this approximation is only valid for head-to-underlayer separations of $d/g > 0.5$. The only satisfactory theoretical treatment available to this boundary value problem is for symmetrical, right-angled corner heads, and involves solutions in the form of infinite Fourier series [11]. The coefficients of the Fourier series solution are determined implicitly from the numerically intensive solution of a truncated, infinite system of linear equations with terms requiring numerical integration. Their study [11] also highlighted that the approximation of using the surface potential or field in the absence of the underlayer represent only the first-order term of the complete and accurate solution for this problem. For asymmetrical heads, only a conformal mapping solution was derived for rational corner angles [9], which also requires numerical inversion. In here, a simplified and explicit general theoretical treatment of this boundary value problem is presented to determine the effect of an underlayer on the surface potential of an arbitrary head structure, requiring only the functional description of the surface potential in the absence of the underlayer.

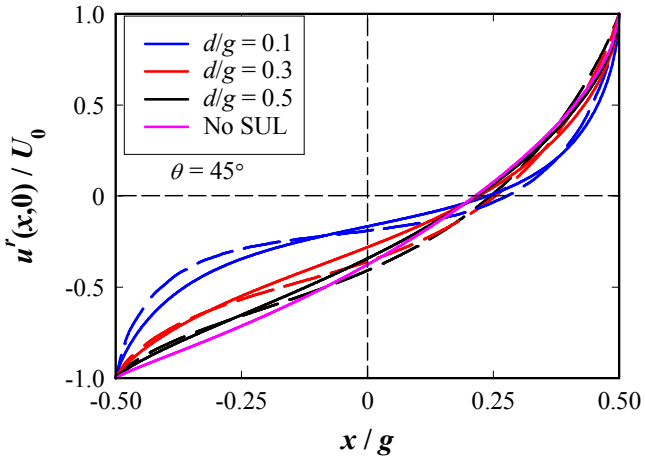

Fig.. 5 Normalised surface potential for an asymmetrical head with corner angle of 45° in the presence of a SUL, calculated using finite-elements (solid lines) and using the Fourier integral transform approximation in this paper (dashed lines). The surface potential without a SUL, calculated using finite-elements, is shown for comparison.

The theoretical treatment starts by assuming the simplified, two-region, boundary value problem shown in Fig. 6 to represent the gap region of a general magnetic head (in region 1) at close proximity d to a SUL beyond the head surface (region 2). The geometry of this model is similar to the 'slot' approximation proposed in [22] for the symmetrical ring-head, but generalised here to model any gapped head structure using the integral transform approach. To simplify the mathematical development and to a very good approximation for small head-to-underlayer separations, the potential on either side of the gap corners is assumed to vary linearly between the head and underlayer, and vanishes at the SUL surface ($y = d$) as indicated in Fig. 6.

This article has been accepted for publication in a future issue of this journal, but has not been fully edited. Content may change prior to final publication. Citation information: DOI 10.1109/TMAG.2015.2492947, IEEE Transactions on Magnetics

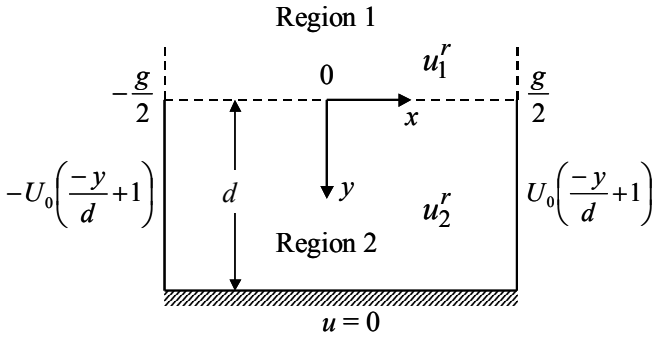

Fig. 6 Theoretical boundary value problem of the gap region for a general magnetic head with arbitrary surface potential distribution a distance *d* from a SUL, used to derive a closed form distribution of the resulting surface potential in response to the SUL. Region 1 represents the magnetic head gap/surface, and Region 2 is the area beyond the head surface.

Solving Laplace's equation through variable separation in Region 2 (beyond the head surface) subject to the boundary conditions indicated in Fig. 6, yields the following Fourier series solution for the potential in the presence of an underlayer:

$$u_2^r(x,y) = U_0\frac{2x}{g}\left(\frac{-y}{d}+1\right) + \sum_{m=1}^{\infty} B_m \sin\left(\kappa_m(x-g/2)\right)\left[e^{-\kappa_m y} - e^{\kappa_m(y-2d)}\right] \tag{4}$$

defined over $-g/2 \le x \le g/2$, where the eignvalues $\kappa_m = m\pi/g$ satisfy the boundary conditions, and the eigenfunctions $\sin\left(\kappa_m(x-g/2)\right)$ were chosen to include translation along the *x*-axis to account for even and odd harmonics in the solution to describe the asymmetry in potential while satisfying the boundary conditions.

In Region 1, the magnetic head potential is assumed to have the general Fourier series solution:

$$u_1^r(x,y) = \phi(x,y) + \sum_{m=1}^{\infty} A_m \sin\left(\kappa_m(x-g/2)\right)e^{\kappa_m y} \tag{5}$$

over the gap region $-g/2 \le x \le g/2$, where $\phi(x,y)$ is the head potential distribution in the absence of the underlayer, satisfying the boundary conditions indicated in Fig. 6 at the head surface. The second, translated Sine series term in (5) models the reaction of the underlayer and represents a series of correction terms to the potential $\phi(x,y)$, with coefficients A_m that are functions of the corner angle θ and head-to-underlayer separation *d*. Again, the translated eigenfunctions are chosen to model the asymmetry in the potential and, together with the eignvalues $\kappa_m = m\pi/g$, satisfy the boundary conditions at the interface *y* = 0. The assumed *y*-dependence in the Fourier series term in (5) follows the exponential decay of fields and potentials expected inside two-dimensional permeable head structures.

The coefficient A_m and B_m in (4) and (5) are determined by forcing continuity of the potentials (i.e. $\phi_1 = \phi_2$) and normal fields (i.e. $-\partial\phi_1/\partial y = -\partial\phi_2/\partial y$) at the interface *y* = 0. Multiplying the two continuity equations by $\sin\left(\kappa_n(x-g/2)\right)$ and integrating over the gap length $\pm g/2$, noting the orthagonality of the translated Sine function:

$$\int_{x=-g/2}^{g/2} \sin\left(\kappa_m(x-g/2)\right)\sin\left(\kappa_n(x-g/2)\right)dx = \begin{cases} 0 & m \ne n \\ g/2 & m = n \end{cases}$$

yields two algebraic equations, which can be solved exactly to reveal the following Fourier coefficients:

$$A_n = -\bar{\phi}\frac{\left(1+e^{-2\kappa_n d}\right)}{g} - \left[\frac{\partial\bar{\phi}}{\partial y}\right]_{y=0}\frac{\left(1-e^{-2\kappa_n d}\right)}{\kappa_n g} + \frac{\bar{v}}{g/2}\left[1-\frac{1}{2}\left(1+\frac{1}{\kappa_n d}\right)\left(1-e^{-2\kappa_n d}\right)\right] \tag{6a}$$

$$B_n = \frac{\bar{\phi}}{g} - \frac{1}{\kappa_n g}\left[\frac{\partial\bar{\phi}}{\partial y}\right]_{y=0} - \frac{\bar{v}}{g}\left(1+\frac{1}{\kappa_n d}\right) \tag{6b}$$

where the overlines indicate integral transforms defined by:

$$\bar{\phi}(\kappa_n,0) = \int_{x=-g/2}^{g/2}\phi(x,0)\sin\left(\kappa_n(x-g/2)\right)dx \tag{7a}$$

$$\left.\frac{\partial\bar{\phi}(\kappa_n)}{\partial y}\right|_{y=0} = \int_{x=-g/2}^{g/2}\left.\frac{\partial\phi}{\partial y}\right|_{y=0}\sin\left(\kappa_n(x-g/2)\right)dx \tag{7b}$$

$\bar{v}$ is the integral transform of the linear gap potential term at *y* = 0, that evaluates exactly to:

$$\bar{v}(\kappa_n,0) = \int_{x=-g/2}^{g/2}\left(\frac{2U_0 x}{g}\right)\sin\left(\kappa_n(x-g/2)\right)dx = -\frac{U_0}{\kappa_n}\left[1+(-1)^n\right] \tag{8}$$

To maintain consistency with the geometry in Fig. 6, $\partial\bar{\phi}/\partial y$ in (6) is determined from the Fourier integral transform of Laplace's equation as detailed in the Appendix. This provides the integral transform of the derivative of the surface potential as:

$$\left.\frac{\partial\bar{\phi}}{\partial y}\right|_{y=0} = -\kappa_m(\bar{\phi}-\bar{v}) \tag{9}$$

which upon substitution in (6) yields the simplified Fourier coefficients:

This article has been accepted for publication in a future issue of this journal, but has not been fully edited. Content may change prior to final publication. Citation information: DOI 10.1109/TMAG.2015.2492947, IEEE Transactions on Magnetics

$$A_n = \frac{-2e^{-2\kappa_n d}}{g}\left(\bar{\phi} - \bar{v}\right) + \frac{\bar{v}}{g\kappa_n d}\left(e^{-2\kappa_n d} - 1\right) \tag{10a}$$

$$B_n = \frac{2}{g}\left(\bar{\phi} - \bar{v}\right) - \frac{\bar{v}}{g\kappa_n d} \tag{10b}$$

This completes the formal solution of the boundary value problem described in Fig. 6. The closed-form, explicit Fourier series representation of the potentials in (4) and (5) and their coefficients in (10) can be used to model the surface potential and fields of general two-dimensional head structures. Moreover, the potentials in (4) or (5) evaluated at $y = 0$ along with the coefficient in (10) correctly produce the surface potential in the absence of the underlayer in (2) as $d \to \infty$. The Fourier coefficients in (10) are functions of the head-to-underlayer separation d, the exterior corner angle θ (through x_0), and head gap length g. Determination of these coefficients requires only knowledge of the surface potential distribution in the absence of an underlayer, which is normally available.

For the asymmetrical head considered here, the surface potential in the presence of the underlayer can now be determined by substituting $\phi(x,0) = u(x,0)$ from (2) into (4) (or (5)) and evaluating the series coefficients in (10). The integral transform of the surface potential of the asymmetrical head (needed for the evaluation of the coefficients) can be integrated exactly in (7a) and is given by:

$$\begin{aligned}\bar{\phi}(\kappa_n,0) = \frac{gU_0}{2x_0^2}\Big\{&-x_0\left(-1+(-1)^n\right)/\kappa_n \\ &+\left(g^2/4 - x_0^2\right)\left[\sin(\alpha)\left(-\mathrm{Ci}(\alpha)+\mathrm{Ci}(\beta)\right)\right\} \\ &-\cos(\alpha)\left(-\mathrm{Si}(\alpha)+\mathrm{Si}(\beta)\right)\Big]\Big\}\end{aligned} \tag{11}$$

where $\alpha = g\kappa_n(g/2 - x_0)/2x_0$, $\beta = g\kappa_n(g/2 + x_0)/2x_0$, $\bar{v}$ is defined in (8), and Si and Ci are the sine and cosine integrals respectively [23].

Fig. 5 illustrates the calculated surface potential for the asymmetrical head with an underlayer for corner angle $\theta = 45°$ using (4) (or equally (5)) (dashed lines) for different head-to-underlayer separations. There is very good agreement between the approximate potential calculated using (4) or (5) and the finite-element calculations in Fig. 5, with maximum normalised RMSD of about 2.8%, that is consistent for other head corner angles. The rate of convergence of the Fourier coefficients in (10) depends on the head-to-underlayer separation d, and on the corner angle θ. For head-to-underlayer separations of $d/g \geq 0.5$, the coefficients converge rapidly and 20 terms (coefficients) were found sufficient, for any θ, in evaluating the surface potential in (4) (or equally (5)). More terms are necessary for head-to-underlayer separation of $d/g < 0.5$, with up to 40 terms needed for the evaluation of the surface potential ad $d/g = 0.1$ in Fig. 5. The number of required series terms can increase with increasing corner inclination θ, to correctly sample larger gradients (short wavelength behaviour) in the potential and fields at the acute corner.

III. Head Magnetic Fields

The magnetic surface potentials derived in the previous section will now be convolved with the Green's function for the asymmetrical head to determine the potential and fields everywhere beyond the head surface. Determining the magnetic fields directly using the surface fields rather than potentials, however, is easier mathematically with the convolution integrals evaluated only over the gap region (since the surface fields vanish over the infinitely permeable poles). This is the approach adopted in this section. Extensive use will be made of the Fourier transform and its inverse for the derivation of Green's functions and field spectra in this article. The Fourier transform and its inverse are defined, respectively, for the spatial function $f(x)$ by:

$$F(k) = \int_{x=-\infty}^{\infty} e^{-jkx} f(x)\,dx \tag{12a}$$

$$f(x) = \frac{1}{2\pi}\int_{k=-\infty}^{\infty} e^{jkx} F(k)\,dk \tag{12b}$$

where $k = 2\pi/\lambda$ is the wavenumber at wavelength λ.

To derive the appropriate Green's functions for the asymmetrical head, the spatial Fourier transform to Laplace's equation in (1) is first taken to remove the x-dependence of the scalar potential. This yields the ordinary differential equation:

$$\frac{\partial^2 u(k,y)}{\partial y^2} - k^2 u(k,y) = 0 \tag{13}$$

which is solved next for the appropriate boundary conditions in the absence and presence of a SUL.

A. Without underlayer

For this semi-infinite geometry (when $d \to \infty$ in Fig. 1), the boundary conditions are such that there is a prescribed surface potential, $u(k,0)$ at $y = 0$, and a vanishing potential as $y \to \infty$. This yields the classical spacing loss dependence of the potential (and fields) on one side of semi-infinite structures:

$$u(k,y) = u(k,0)e^{-ky} \tag{14}$$

To reduce the complexity of the mathematical derivations, the gradient of the potential in (14) is taken to produce the Fourier transforms of the magnetic fields, i.e.:

This article has been accepted for publication in a future issue of this journal, but has not been fully edited. Content may change prior to final publication. Citation information: DOI 10.1109/TMAG.2015.2492947, IEEE Transactions on Magnetics

$$H_x(k,y) = H_x(k,0)e^{-ky} \tag{15a}$$

$$H_y(k,y) = j\,\mathrm{sgn}(k)H_x(k,0)e^{-ky} \tag{15b}$$

where H_x and H_y are the x- and y-components of the magnetic field respectively, $H_x(k,0)$ is the Fourier transform of the x-component of the surface field, and sgn is the Signum function. Taking the inverse Fourier transform of (15) and invoking the convolution theorem of Fourier transforms yields the magnetic fields beyond the head surface:

$$H_x(x,y) = \frac{y}{\pi}\int_{x'=-\infty}^{\infty} \frac{H_x(x',0)}{(x'-x)^2 + y^2}\,dx' \tag{16a}$$

$$H_y(x,y) = \frac{-1}{\pi}\int_{x'=-\infty}^{\infty} \frac{H_x(x',0)(x'-x)}{(x'-x)^2 + y^2}\,dx' \tag{16b}$$

For the asymmetrical head considered in this work, the magnetic field along the head surface is determined from the gradient of the surface potential in (2) which is given by:

$$H_x(x,0) = \frac{-\partial u(x,0)}{\partial x} = \frac{-gU_0}{2}\frac{(g^2/4 - x_0^2)}{(g^2/4 - x_0 x)^2} \tag{17}$$

Substituting (17) into (16a), and integrating over the gap length yields exactly the x-component of the magnetic field everywhere beyond the head surface as:

$$\begin{aligned} H_x(x,y) = {} & \frac{-g^2 H_0}{4\pi}\left\{\frac{x_0^2 y}{g/4\left((g^2/4 - x_0 x)^2 + x_0^2 y^2\right)}\right. \\ & + \frac{\left(g^2/4 - x_0^2\right)}{\left(\left(g^2/4 - x_0 x\right)^2 + x_0^2 y^2\right)^2} \\ & \times\left[h_x^k(x,y)\left(\left(g^2/4 - x_0 x\right)^2 - x_0^2 y^2\right)\right. \\ & \left.\left. + x_0 y\left(g^2/4 - x_0 x\right)\left[h_y^k(x,y) + \ln\left(\frac{(g/2 + x_0)^2}{(g/2 - x_0)^2}\right)\right]\right]\right\} \end{aligned} \tag{18}$$

while substituting (17) into (16b) yields exactly the y-component of the magnetic field as:

$$\begin{aligned} H_y(x,y) = {} & \frac{-g^2 H_0}{2\pi}\left\{\frac{-x_0\left(g^2/4 - x_0 x\right)}{g/2\left(\left(g^2/4 - x_0 x\right)^2 + x_0^2 y^2\right)}\right. \\ & + \frac{\left(g^2/4 - x_0^2\right)}{\left(\left(g^2/4 - x_0 x\right)^2 + x_0^2 y^2\right)^2} \\ & \times\left[x_0 y\left(g^2/4 - x_0 x\right)h_x^k(x,y) - \frac{1}{4}\left(\left(g^2/4 - x_0 x\right) - x_0^2 y^2\right)\right. \\ & \left.\left.\left[h_y^k(x,y) + \ln\left(\frac{(g/2 + x_0)^2}{(g/2 - x_0)^2}\right)\right]\right]\right\} \end{aligned} \tag{19}$$

where:

$$h_x^k(x,y) = \tan^{-1}\left(\frac{x + g/2}{y}\right) - \tan^{-1}\left(\frac{x - g/2}{y}\right)$$

and

$$h_y^k(x,y) = \ln\left[\frac{(x - g/2)^2 + y^2}{(x + g/2)^2 + y^2}\right]$$

are the normalised field components for the symmetrical (right-angled) head with linear gap potential (Karlqvist approximations), and $H_0 = 2U_0/g$ is the x-component of the deep-gap field. The first terms on the right-hand-side of (18) and (19) describe the increase in surface charge density on the right corner with increasing exterior angle θ, and correctly yield the narrow gap fields as $\theta \to 90^o$ (and $x_0 \to g/2$). Similarly, equations (18) and (19) correctly reduce to the Karlqvist field approximations when the head is symmetrical at $\theta = 0^o$ (and hence $x_0 = 0$). Moreover, examination of equations (18) and (19) reveal that the fields of asymmetrical heads (in the absence of an underlayer) may approximately be constructed from a weighted sum of the x and y components of the magnetic fields of the symmetrical (right-angled) head and the narrow gap head, where the weights are functions of the exterior corner angle θ.

The x and y field components for the asymmetrical head are plotted in Fig. 7 for different corner angles at $y/g = 0.05$, calculated using equations (18) and (19) (dashed lines) and compared with the finite-element calculations from Comsol Multiphysics® (solid lines). Fig. 7 shows the increase in asymmetry in both H_x and H_y with increasing θ, resulting from the increase in surface charge density and potential gradient near the acute corner of the head ($x = g/2$) with increasing θ. The increased asymmetry leads to reduction in the effective head gap length towards the right corner ($x_0 \to g/2$), consequently causing the increase in the magnitude of the fields and narrowing of their distributions in this region.

This article has been accepted for publication in a future issue of this journal, but has not been fully edited. Content may change prior to final publication. Citation information: DOI 10.1109/TMAG.2015.2492947, IEEE Transactions on Magnetics

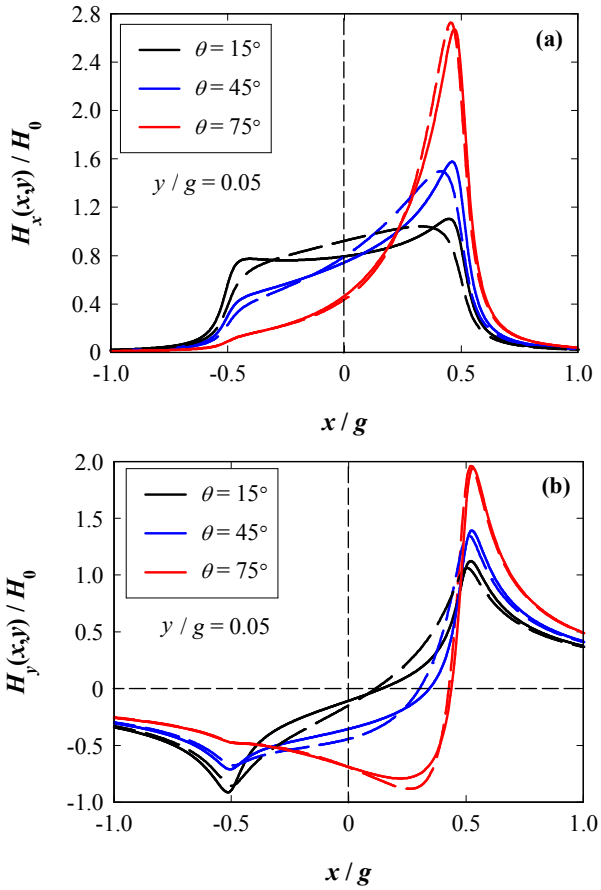

Fig. 7 (a) Normalised x-component of the magnetic field, and (b) normalised y-component of the magnetic field for the asymmetrical head in the absence of a SUL for different exterior corner angles θ, calculated using finite-elements (solid lines) and using the approximate models in equations (18) and (19) (dashed lines). The fields were calculated in close proximity to the head surface at $y/g = 0.05$.

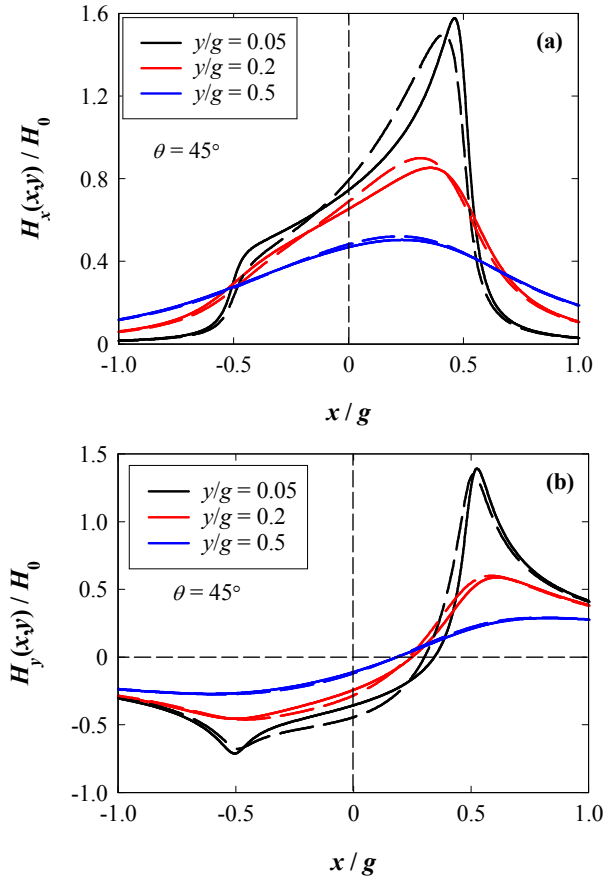

Fig. 8 (a) Normalised x field component, and (b) y field component for the asymmetrical head in the absence of a SUL for exterior corner angle $\theta = 45°$, calculated using finite-elements (solid lines) and using the approximate models in equations (18) and (19) (dashed lines) for increasing spacing y/g from the head surface.

The approximate fields calculated using (18) and (19) correctly capture the asymmetry in the magnetic fields and dependence of both magnitude and distribution on exterior corner angle θ as illustrated in Fig. 7 (dashed lines), with some deviation from the finite-element calculations near the centre of the gap and corners for small values of θ. For H_x in Fig 7(a), the normalised RMS deviation between the approximate and finite-element calculations is largest at 9% for $\theta = 15°$, reducing to 6% for $\theta = 45°$, and decreasing further to 1.7% for $\theta = 75°$. Fig. 7(b) shows that the approximate H_y generally exhibits closer agreement with the finite-element calculations with normalised RMSD of 5% for $\theta = 15°$, reducing to 4.5% for $\theta = 45°$, and down to 1.7% for $\theta = 75°$. This reduction of error in the approximate fields with increasing θ is consistent with the reduction in the error of the derived surface potential in (2) with increasing θ as illustrated in Fig. 4. The largest RMS deviation at small value of θ is in line with the accuracy expected of the linear (Karlqvist) gap potential approximation for symmetrical heads where the contribution of the magnetic charges on the pole surfaces is underestimated [24].

At increasing distances from the head surface, the magnetic fields decrease in amplitude and their distributions broaden as illustrated in Fig. 8. The increase in y/g is accompanied by increased agreement between the approximate fields calculated using (18) and (19) and the finite-element calculations as demonstrated in Fig. 8, for $\theta = 45°$ as a representative example. The normalised RMSD between the approximate and exact (finite-element) H_x is 6% for $y/g = 0.05$ and reduces to 1.6% for $y/g = 0.5$. Similarly, the normalised RMSD for H_y continues the decrease with increasing θ at 4.5% for $y/g = 0.05$, and down to 1% for $y/g = 0.5$.

B. With underlayer

In the presence of a SUL, the particular solution of Laplace's equation in (13) subject to a prescribed potential u^r (function of the head-to-underlayer spacing d and corner angle θ) at $y = 0$, and a vanishing potential at the surface of the underlayer ($y = d$), was found to be:

$$u^r(k,y) = -u^r(k,0)\frac{\sinh(k(y-d))}{\sinh(kd)} \tag{20}$$

This article has been accepted for publication in a future issue of this journal, but has not been fully edited. Content may change prior to final publication. Citation information: DOI 10.1109/TMAG.2015.2492947, IEEE Transactions on Magnetics

Thereafter, the superscript '*r*' will be used to indicate potentials and fields in the presence of a SUL. Following the analysis of the previous section, it is more convenient mathematically to work with magnetic fields rather then potentials, and therefore the gradient of the potential in (20) is taken to produce the Fourier transform of the magnetic fields:

$$H_x^r(k,y) = -H_x^r(k,0)\frac{\sinh(k(y-d))}{\sinh(kd)} \tag{21a}$$

$$H_y^r(k,y) = jH_x^r(k,0)\frac{\cosh(k(y-d))}{\sinh(kd)} \tag{21b}$$

where $H_x^r(k,0)$ is the surface field transform. Evaluating the inverse Fourier transforms of (21) using the convolution property of Fourier transforms yields the convolution integrals:

$$H_x^r(x,y) = \frac{-1}{2d}\int_{x'=-\infty}^{\infty}\frac{\sin(\pi y/d)H_x^r(x',0)}{\cos(\pi y/d)-\cosh(\pi(x'-x)/d)}dx' \tag{22a}$$

$$H_y^r(x,y) = \frac{1}{2d}\int_{x'=-\infty}^{\infty}\frac{H_x^r(x',0)\sinh(\pi(x'-x)/d)}{\cos(\pi y/d)-\cosh(\pi(x'-x)/d)}dx' \tag{22b}$$

The field expressions in (22) account for the infinite reflections of the magnetic fields between the high permeability head surface and underlayer [21], and the effect of the gap and the reaction of the underlayer on the surface field are included in the surface field $H_x^r(x,0)$. For the asymmetrical head considered here, the surface field $H_x^r(x,0)$ can be derived from the gradient of the potential in (9) (or equally (10)). Choosing (9) due to the mathematical simplicity of the first linear term in the expression, and evaluating the derivative with respect to x yields the surface field:

$$H_x^r(x,0) = -H_0 - \sum_{m=1}^{\infty}\kappa_m B_m \cos(\kappa_m(x-g/2))(1-e^{-2\kappa_m d}) \tag{23}$$

where $H_0 = 2U_0/g$, and the coefficient B_m are given explicitly in (10b). It is possible to integrate (22) exactly using the surface field distribution in (23), however the solution is intractable and in terms of the hypergeometric series function. The magnetic fields in (22) can be numerically evaluated more conveniently and quickly using the inverse Fast Fourier Transform from equations (21). Alternatively, and in this article, the fields in (22) were more easily integrated numerically over the gap length using the surface field in (23).

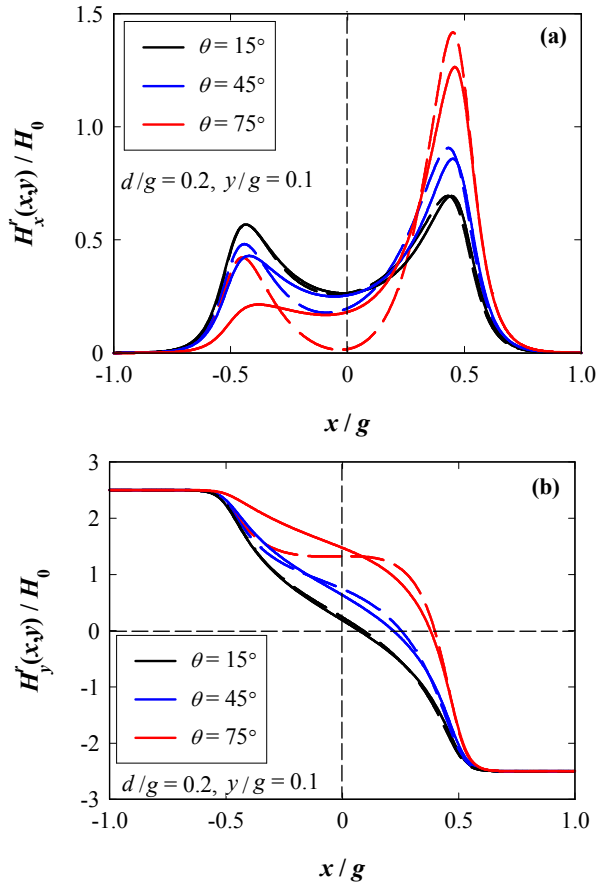

Fig. 9 (a) Normalised x field component, and (b) y field component for the asymmetrical head in the presence of a SUL for different corner angles θ, calculated for a head-to-underlayer separation d/g = 0.2 at distance y/d = 0.1 from the head surface. Solid lines are the finite-element calculations, and the dashed lines are from the theoretical model in (22) and using the surface field distribution from (23).

Fig. 9 shows the magnetic fields for the asymmetrical head for different degrees of corner asymmetry with head-to-underlayer separation d/g = 0.2, calculated at a head spacing y/g = 0.1 using finite elements (straight lines) and the theoretical models in (22) and (23) (dashed lines). The presence of the soft underlayer enhances H_y at the expense of H_x, with H_x confined to the pole corners as indicated in Fig. 9(a). Following a similar pattern to the head fields without an underlayer, the increase in the exterior corner angle θ increases the asymmetry in the magnetic fields in general, and particularly increases the magnitude of H_x near the acute corner (at $x = g/2$). With increases in θ, the zero-crossing in H_y shifts towards the right corner as shown in Fig. 9(b) following the shift in the surface potential. Beyond the head corners and over the pole regions, H_y tends to a constant magnitude that depends only on the ratio of d/g as demonstrated in Fig. 9(b). This dependence can be easily derived from (22b) by evaluating the limit $x \to \pm\infty$, thus reducing the convolution integral to $1/2d\int_{x'=-g/2}^{g/2} H_x^r(x',0)dx'$. Substitution of (23) and integration yields the constant normalised field $H_y^r/H_0 \approx \pm g/2d$ (i.e. H_y over the head

This article has been accepted for publication in a future issue of this journal, but has not been fully edited. Content may change prior to final publication. Citation information: DOI 10.1109/TMAG.2015.2492947, IEEE Transactions on Magnetics

poles is determined by the first, long wavelength, term of the surface field in (23)).

The normalised RMS deviation between H_x^r calculated using (22a) and the finite-element calculations is small at 2.5% for θ = 15°, and increases to 4.5% for θ = 45°, and reaches 7% for θ = 75°. The approximate H_y^r again exhibits closer agreement with the finite-element calculations as indicated in Fig. 9(b), particularly for small exterior corner angles with normalised RMS deviation of 0.7% when θ = 15°. The deviation however increases to 1.5% for θ = 45°, and is 4.4% with when θ = 75°. The deviation of the approximate field models from the accurate finite-element calculations in Fig. 9 is mainly confined to the central region of the gap. This is where the surface potential expressions in (4) or (5), derived based on the approximate boundary value problem described in Fig. 6, predict a lower surface potential gradient (see Fig. 5) and therefore fields in that region compared to the finite-element solution. This is caused by the use of the approximate expression for the normal derivative of the surface potential in (9) for the evaluation of the series coefficients. This deviation can be reduced by using a more accurate expression for the normal derivative of the surface potential in evaluating the coefficients in (6) (determined from (19) for example). However, care must be exercised in this case since the resulting surface potential will not be consistent with the boundary value problem in Fig. 6, with expected derivations from the correct solution near the gap corner regions.

The dependence of the magnetic fields on the head-to-underlayer separation is depicted in Fig. 10 for a fixed corner angle θ = 45°. For small d/g < 0.5, H_x^r is confined and have maxima near the head corners as indicated in Fig. 10(a). Increasing the head-to-underlayer separation enhances the magnitude of H_x^r at the acute pole corner, and beyond d/g > 0.5 causes only modest changes to the magnetic fields as they become comparable to the fields without an underlayer. The normalised RMS derivation between the approximation in H_x^r and finite-element calculations starts at 5% for d/g = 0.2, and reduces to 4% with increased head-to-underlayer spacing at d/g = 1. For increasing values of d/g > 0.5, H_y^r decreases in amplitude, and the fields beyond the pole corners fall to zero following the behaviour of the fields in the absence of the underlayer as indicated in Fig. 10(b). The RMS deviation between the approximate and exact H_y^r fields in this case is 1.5% at d/g = 0.2 and increases to 2.7% for d/g = 1 in line with the previously estimated RMS deviation values in the absence of the underlayer.

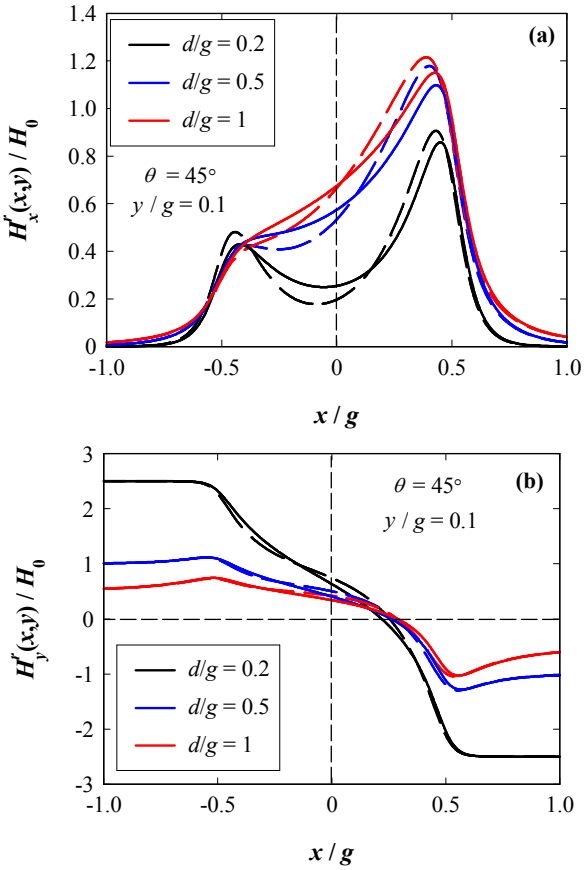

Fig. 10 (a) Normalised x field component, and (b) y field component for the asymmetrical head in the presence of a SUL, for exterior corner angle θ = 45°. Solid lines are for the finite-element calculations, and the dashed lines are from the theoretical model in (22) and using the surface field from (23).

IV. Fourier Transform Of Surface Fields

The magnetic fields everywhere beyond the head surface were determined in Section 3 from the convolution of the head surface field with the Green's function for the two-dimensional geometry indicated in Fig. 1. In particular equations (15) and (21) show that the wavelength content of the magnetic fields is primarily determined by the Fourier transform of the surface field, before being filtered by spacing losses when moving away from the head surface. Thus the surface field transform provides details on the wavelength content of the magnetic fields without any spacing losses, and will be determined next for the asymmetrical head in the presence and absence of a SUL. These surface field transforms are also valuable for the numerical evaluation of the magnetic fields using the inverse Fourier transform.

A. Without underlayer

The x-component of the magnetic field along the surface of the asymmetrical head is derived from the gradient of the potential in (2) and is given in (17). The surface field in (17) reveals the two connected characteristics of the surface

This article has been accepted for publication in a future issue of this journal, but has not been fully edited. Content may change prior to final publication. Citation information: DOI 10.1109/TMAG.2015.2492947, IEEE Transactions on Magnetics

potential and fields for asymmetrical heads: namely the shift of the zero-crossing of the potential and therefore field locations with the change in corner angle θ (through x_0), and the scaling of x-axis by x_0 which affects the magnitude and the width of the distribution of the fields with the change in θ. Both of these effects contribute to the reduction of effective gap length and narrowing of field distributions towards the acute head corner, as illustrated previously.

Evaluating the Fourier transform (defined in (12a)) of the surface field in (17) yields:

$$H_x(k,0) = \frac{-gH_0}{2x_0}\left\{\left[-2x_0\cos\left(\frac{kg}{2}\right)+jg\sin\left(\frac{kg}{2}\right)\right] + j\frac{kg}{2x_0}\left(\frac{g^2}{4}-x_0^2\right)e^{\frac{-jkg^2}{4x_0}} \times\left[\mathrm{Ei}\left(j\frac{kg}{2x_0}\left(\frac{g}{2}-x_0\right)\right)-\mathrm{Ei}\left(j\frac{kg}{2x_0}\left(\frac{g}{2}+x_0\right)\right)\right]\right\} \quad (24)$$

where Ei is the exponential integral function [23]. The Fourier transform in (24) is complex due to the asymmetrical nature of the fields. Figure 11 shows the calculated magnitude of the Fourier transform in (24) for different exterior corner angles. At θ = 0°, the spectrum is the well-known Sinc function describing the Fourier transform of the constant (Karlqvist) surface field over the gap region, with nulls at exact multiples of the gap length. Increasing the exterior angle θ reduces the effective gap length of the head and narrows the field spatial distribution, therefore increasing the magnitude of the spectrum at shorter wavelengths (higher k), and diluting the gap nulls. The broadening of the spectrum continues with increasing θ until the narrow gap (or far field) limit is attained at θ = 90°, corresponding to infinitely small gap length and infinitely narrow surface field distribution, which is represented by the constant spectrum in Fig. 11.

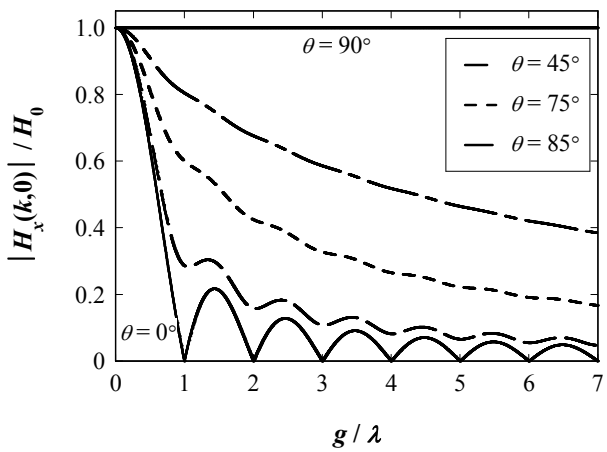

Fig. 11 Normalised head surface field transform for the asymmetrical head (in the absence of an underlayer) as a function of exterior corner angle θ. The solid lines show the spectra of symmetrical heads including the Karlqvist head (θ = 0°) and the narrow gap head (θ = 90°).

B. With underlayer

The presence of a soft underlayer causes an enhancement of H_y^r, making it of practical importance for magnetic recording. Nevertheless, the x-component of the surface field $H_x^r(k,0)$ still decides the surface wavelength spectrum of H_y^r as indicated by equation (21b). Convolving $H_x^r(k,0)$ with the low-pass filter term 1/tanh(kd) in (21b) further enhances the short wavelengths in the spectrum therefore increasing the magnitude of H_y^r over the head poles with reduction in head-to-underlayer separation d as shown in Fig. 10(b). $H_x^r(k,0)$ can be determined from the gradient of (4) (or equally (5)) at y = 0. For mathematical convenience, the surface field in (23) will be used again, with Fourier transform given by:

$$H_x^r(k,0) = -gH_0\frac{\sin(kg/2)}{(kg/2)} - 2k\sum_{m=1}^{\infty} j^m\kappa_m B_m(1-e^{-2\kappa_m d})\frac{\sin\left(g/2(k+\kappa_m)\right)}{k^2-\kappa_m^2} \quad (25)$$

The surface field spectrum in (25) follows the same dependence on exterior corner angle θ as that indicated in Fig. 11 in the absence of an underlayer, and will not be illustrated here. Specifically, the width and therefore wavelength content of the spectrum in (25) also increases with increasing θ, due to the reduction in effective gap and narrowing of field distributions. The effect of the head-to-underlayer spacing on head surface transform in (25) is illustrated in Fig. 12 for θ = 45°. Reducing the head-to-underlayer separation results in displacement of the gap-nulls toward larger wavelengths (smaller k) and increases in the amplitude of the ripples in the spectrum. This behaviour persists for all other corner angles.

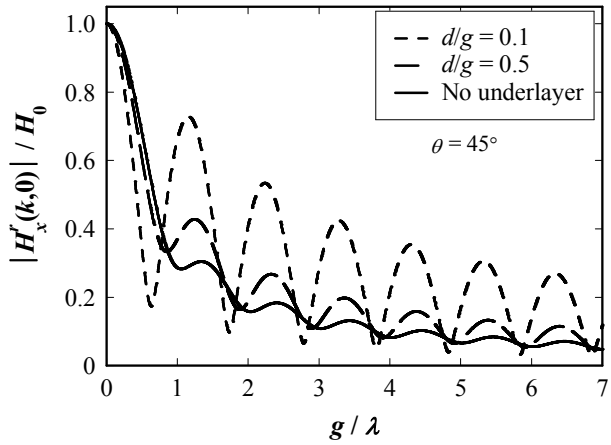

Fig. 12 Normalised head surface field transforms for an asymmetrical head in the presence of an underlayer for θ = 45° at different head-to-underlayer spacings.

This article has been accepted for publication in a future issue of this journal, but has not been fully edited. Content may change prior to final publication. Citation information: DOI 10.1109/TMAG.2015.2492947, IEEE Transactions on Magnetics

V. Summary and Conclusions

This article provided a closed-form approximate model for the surface magnetic potential of the asymmetrical head in two-dimensions, demonstrating very good agreement with two-dimensional finite-element calculations, for a wide range of exterior corner angles from 0° (rectangular head) to 90° (narrow gap head). The theory is two-dimensional and assumes infinite track-width heads, and based on the static scalar magnetic potential and therefore ignores head transients. Moreover, pole corner and SUL saturation effects were neglected in this approximate and analytical treatment.

A general analytical theory was developed to model the reaction of a soft magnetic underlayer on the surface potential of any two-dimensional head structure. This theory was applied to the asymmetrical head and predicted, to very good agreement with finite-element calculations, the surface potential and fields from asymmetrical heads as functions of head corner angle and head-to-underlayer separation.

The analytical models for the surface potential with and without an underlayer were convolved with the two-dimensional Green's function for the asymmetrical head to derive relatively simple closed-form expressions for the magnetic fields beyond the surface of asymmetrical heads. The approximate magnetic fields were in very good agreement with finite-element calculations over a wide range of corner inclination angles and head-to-underlayer separations. The analytical expressions revealed that the magnetic fields from asymmetrical heads may be derived from a weighted sum of the horizontal and vertical field components.

Exact expressions for the Fourier transforms of the asymmetrical head surface fields were also derived, correctly demonstrating the increase in the wavelength content of the field spectrum with increasing exterior corner angle (due to the reduction in effective gap length and narrowing of the field distributions).

The theory presented here can be used to evaluate the magnetic fields of two-dimensional head structures with multiple asymmetrical gaps, and easily incorporated into numerical studies of magnetic recording with minimum computational effort.

Appendix

Solution of Laplace's equation using the translated Sine transform

Laplace's equation in two-dimensions for the scalar magnetic potential ϕ for the geometry shown in Fig. 6 in the absence of the underlayer (i.e. $d \to \infty$) is given by:

$$\frac{\partial^2 \phi}{\partial x^2} + \frac{\partial^2 \phi}{\partial y^2} = 0$$

Taking the translated Sine integral transform of Laplace's equation, defined for $\phi(x,y)$ as:

$$\bar{\phi}(\kappa_n, y) = \int_{x=-g/2}^{g/2} \phi(x, y) \sin\left(\kappa_n (x - g/2)\right) dx$$

and applying successive integration by parts, observing the boundary conditions indicated in Fig. 6 with eignvalues $\kappa_n = n\pi / g$, reduces Laplace's equation to the ordinary differential equation:

$$\frac{\partial^2 \bar{\phi}}{\partial y^2} - \kappa_n^2 \left(\bar{\phi} - \bar{v}\right) = 0 \qquad \text{(A.1)}$$

where the eignvalues $\kappa_n = n\pi / g$ and eigenfunctions $\sin(\kappa_n (x - g/2))$ satisfy the boundary conditions shown in Fig. 6, and allow asymmetrical description of $\phi(x,0)$ in the transform. $\bar{v}$ is the integral transform of the linear gap potential at $y = 0$, and is defined by:

$$\bar{v}(\kappa_n, 0) = \int_{x=-g/2}^{g/2} \left(\frac{2U_0 x}{g}\right) \sin\left(\kappa_n (x - g/2)\right) dx$$

The general solution to (A.1) is given by:

$$\bar{\phi}(\kappa_n, y) = Ce^{\kappa_n y} + De^{-\kappa_n y} + \bar{v} \qquad \text{(A.2)}$$

where C and D are the constants of the integration. Application of the boundary conditions that $\bar{\phi}$ vanishes as $y \to \infty$, with prescribed surface potential $\bar{\phi}(\kappa_n, 0)$ at $y = 0$ yields the particular solution of (A.2) as:

$$\bar{\phi}(\kappa_n, y) = \left(\bar{\phi}(\kappa_n, 0) - \bar{v}\right) e^{-\kappa_n y} + \bar{v} \qquad \text{(A.3)}$$

The normal derivative of the integral transform of the potential is therefore given by:

$$\frac{\partial \bar{\phi}(\kappa_n, y)}{\partial y} = -\kappa_n \left(\bar{\phi}(\kappa_n, 0) - \bar{v}\right) e^{-\kappa_n y} \qquad \text{(A.4)}$$

REFERENCES

[1] B. K. Middleton, "*Recording and Reproducing Processes*", in Magnetic Recording, Volume I: Technology, Editors: C. D. Mee and E. D. Daniel, Chap. 2, McGraw-Hill, 1987.

[2] J. D. Jackson, "*Classical Electrodynamics*", 3rd Ed., John Wiley & Sons Ltd., Chap 2, Sec. 2.11, p. 75, 1999.

[3] C. S. Wang and H. L. Huang, "Characteristics of asymmetric heads," J. Phys. Colloques 49, C8-2023, 1988.

[4] C. S. Wang and H. L. Huang, "Gap-null free spectral response of asymmetric ring heads for longitudinal and perpendicular recording," IEEE Trans. Magn., Vol. 26(5), 2403, 1990.

[5] Y. Kanai, R. Matsubara, H. Watanabe, H. Muraoka, and Y. Nakamura, "Recording field analysis of narrow-track SPT head with side shields, tapered main pole, and tapered return path for 1 Tb/in^2," IEEE Trans. Magn., Vol. 39 (10), 1955, 2003.

[6] R. H. Victora, S. M. Morgan, K. Momsen, E. Cho, and M. F. Erden, "Two-dimensional magnetic recording at 10Tbits/in^2," IEEE Trans. Magn., Vol. 48(5), 1697, 2012.

[7] J. Yang and C. Chang, "Exact field calculations for asymmetric ring heads," IEEE Trans. Magn., Vol. 28(5), 2072, 1992.

[8] J. Yang and C. Chang, "Magnetic field of an asymmetric ring head with an underlayer," IEEE Trans. Magn., Vol. 29(2), 2069, 1993.

[9] G. J. Y. Fan, "A Study of the playback process of a magnetic ring head," IBM J. of Res. & Dev. 5, 321, 1961.

[10] D. T. Wilton, "An analysis of the magnetic field of a ring head with a highly permeable underlayer," IEEE Trans. Magn., Vol. 27(4), 3751, 1991.

[11] G. J. Y. Fan, "Analysis of a practical perpendicular head for digital purposes," J. Appl. Phys., Supplement To Vol. 31(5), 402S-403S, 1960.

[12] H. A. Shute, D. T. Wilton, and D. J. Mapps, "Analytic field components for perpendicular thin-film recording heads," IEEE Trans. Magn., Vol. 37(6), 3947, 2001.

[13] S. J. C. Brown, D. T. Wilton, H. A. Shute, and D. J. Mapps, "Analytic solutions for double-element shielded magnetoresistive heads," IEEE Trans. Magn., Vol. 35(5), 4339, 1999.

[14] D. T. Wilton, B. K. Middleton, and M. M. Aziz, "Exact harmonic coefficients for a magnetic ring head," IEEE Trans. Magn., Vol. 35(3), 2043, 1999.

[15] O. Karlqvist, "Calculation of the magnetic field in the ferromagnetic layer of a magnetic drum," Trans. Roy. Inst. Techno., Stockholm, No. 86, 3-27, 1954.

[16] T. J. Szczech, and P. R. Iverson, "An approach for deriving field equations for magnetic heads of different geometrical configurations," IEEE Trans. Magn., Vol. 22(5), 355, 1986.

[17] http://www.comsol.com/comsol-multiphysics

[18] H. N. Bertram and C. W. Steele, "Pole tip saturation in magnetic recording heads," IEEE Trans. Magn., Vol. 12(6), 702, 1976.

[19] H. L. Huang, T. Y. Lee, and Y. Huang, "Saturation effects on read/write characteristics of asymmetric ring head," IEEE Trans. Magn., Vol. 28(5), 2650, 1992.

[20] H. N. Bertram, "*Theory of Magnetic Recording*", Cambridge University Press, Cambridge, 1994.

[21] D. S. Bloomberg, "Spectral response from perpendicular media with gapped head and underlayer," IEEE Trans. Magn., Vol. 19(4), 1493, 1983.

[22] D. T. Wilton, H. A. Shute and D. J. Mapps, "Accurate approximation of fields and spectral response functions for perpendicular recording heads," IEEE Trans. Magn., Vol. 35(4), 2172, 1999.

[23] M. Abramowitz and I. Stegun, "*Handbook of Mathematical Functions*", National Bureau of Standards, Tenth printing, p. 231, 1972.

[24] J. J. M. Ruigrok, "*Short-Wavelength Magnetic Recording: New Methods And Analyses*", Elsevier Advanced Technology, Oxford, 1990.